Noname manuscript No.
(will be inserted by the editor)

A Quantitative Study of the Dynamic Response of Soft Tubing for Pressure-driven Flow in a Microfluidics Context

Marie Hébert · William Baxter · Jan P. Huissoon · Carolyn L. Ren

Received: date / Accepted: date

Abstract Microfluidics typically uses either a syringe pump that regulates the flow rate in microchannels or a pressure pump that controls the inlet pressures to drive the flow. In the context of pressure-driven flow, a reservoir holder containing liquid samples is normally used to interface the pressure pump with the microfluidic chip via soft tubing. The tubing connecting the pump and holder transports the pressurized air while the tubing connecting the holder and chip transports the liquid samples. The pressure output from the pump is usually assumed to be stable and the same as that applied to the liquid in the chip; however, in practice this assumption is often incorrect and may negatively impact chip performance. This assumption is critically challenged when applied to microfluidic chips involving dynamic control of fluids since the pressures are constantly varied (at $>$ 10 Hz). This study presents a method for investigating, quantifying and modelling the pump stability and the dynamics of the air tubing using two pressure sensors. The relationship between the pressure output from the pump and the reservoir holder pressure is generalized as a first-order linear system. This relationship allows the software that controls the pressure pump to output the required pressure to the reservoir holder and thus to the microfluidic chip. These results should significantly improve the performance of microfluidic chips using active fluid control, and may also benefit passive fluid control applications.

Keywords Microfluidics · Active control · Tubing · Dynamic response · Pressure-driven flow

Carolyn L. Ren
Mechanical and Mechatroncis Engineering at University of Waterloo,
200, University Avenue West, Waterloo, Ontario, Canada.
Tel: +1 519 888 4567 x 33030.
E-mail: c3ren@uwaterloo.ca

1 Introduction

1.1 Microfluidics context

Microfluidics deals with fluid flows at the micrometre scale. This enabling technology has been applied in a wide range of fields such as biological assays (Crabtree et al. 2012; Atabakhsh and Ashtiani 2018; Azizi et al. 2019), material synthesis (Wang et al. 2017a, Wang et al. 2017b), biofuels (Bodénès et al. 2019), drug screening Rasponi et al. 2015, and many more. Droplet microfluidics is a subset of microfluidics that considers monodispersed picoliter- to nanoliter-sized droplets as reaction vesicles. The immiscibility of the two phases in combination with good wetting conditions (meaning that one fluid preferably wets the channel surface) allows the isolation of the dispersed phase droplets (typically water) within the continuous phase fluid (typically oil). Hence, the chemical reactions designed to occur in the droplets are confined, minimizing cross contamination and enhancing mixing. Other major advantages of using microfluidics include reduced reagent consumption and shortened reaction time.

Generally, droplet manipulation methods are categorized as either passive or active. Passive approaches generally rely on microchannel network arrangement, geometry, and applied pressures or flow rates to achieve the desired droplet manipulations. Active methods use external forces to better control the fluid. Although there exists a wide variety of methods to drive the flow for both passive and active microfluidic solutions, the syringe pump and pressure pump are the most widely utilized.

A syringe pump is generally more lenient than a pressure pump in terms of microchip design (Glawdel and Ren 2012); however, the performance is compro-

mised due to inherently long-term persistent transient behaviour (Korczyk et al. 2011). Additionally, a pressure pump responds much faster than a syringe pump when a change in setpoint is required (Kieffer et al. 2012); thus, pressure pumps exhibit desirable behaviour both on short and long timescales. The short-term dynamics are especially important for active microfluidics that involves frequent adjustment of the applied pressures to the chip.

1.2 Motivation

A novel method has been developed for active manipulation of droplets in a microfluidic platform without the use of external components such as electrodes (Wong and Ren 2016, Hébert et al. 2019). Central to this method is a controller that calculates the pressures that must be applied to the chip inputs to achieve the desired manipulation of the droplets. This controller design uses a fluid dynamics model to issue pressure pump commands multiple times per second. It requires fast actuation, and a pump that can provide rapid pressure adjustments.

Although a pressure pump provides key advantages for active manipulation of droplets, the associated setup requires an interface between the pressurized air from the pump and the fluid to be driven in the chip; this is achieved by the so-called reservoir holder. Figure 1 schematically represents the setup. Flexible tubing is used to connect the pressure pump outlets to the reservoir inlets to transport the pressurized air. Secondary tubing transports the liquid sample from the reservoir holder outlet to the microfluidic chip. The performance of this active method for droplet manipulation can be challenged due to the dynamic difference between the output pressures specified by the controller and the applied pressures to the chip, $P_{pump,output} \neq P_{chip,input}$. This issue has not been so much of a concern for passive methods, which do not require fast pressure actuation. These dynamic differences in command and actual at-chip pressures are due to a combination of components: the communication between the controller and pump; the response of the pump; the dynamics of the air tubing; and the dynamics of the liquid sample tubing. The communication delay is very small in comparison to the mechanical dynamics, and we assume this is negligible. The liquid sample tubing has a much higher resistance and modulus than the air tubing, and so we assume that this is also negligible (please see supplemental). The dynamic response of the pump is typically in the vicinity of 100ms, and the dynamics of the air tubing are unknown. This study thus focuses on investigating the dynamic behaviour of the air tubing and the pressure pump and quantifying the deviations from the requested pressures and the pressures applied to the chip. Understanding these dynamic behaviours is not only useful to improving the performance of the active controller by including these in the controller model, but also highly beneficial to other active microfluidic methods that involve the use of pressure pumps.

1.3 Literature overview

While there exists pertinent literature, the context differs sufficiently to justify the investigation of the case under study on its own. The two closest comparable applications are transmission lines for unsteady pressure measurement, and blood flow in arteries - these will be elaborated below.

The system of differential equations that accurately describe the physical system is too complex to have a useful analytical solution. The 1mm thick tubing falls within the thick-walled cylinder classification based on its ratio to the inner diameter: $d_i/t_h = 1 < 40$, (Schmid et al. 2013). The relationship between inner pressure and radial strain for thick-walled tubing is available in the literature (Schmid et al. 2013); however, measuring the radial strain of the small tubing (i.e. 1 mm inner diameter and 3 mm outer diameter) is experimentally challenging. Consequently, the experimental approach with two pressure sensors is favoured; the pressure drop over the air tubing can be accurately measured and incorporates the effects of the radial strain.

1.3.1 Transmission lines for unsteady pressure measurement

The dynamic response of transmission lines for pressure measurement is of interest when considering unsteady phenomena. By using a lumped parameter model, the gas is assumed to move as a unit rather than as a wave. The soundness of this assumption can be gauged by comparing the tubing length to the wavelength based on the speed of sound in the medium. Either way, the finite propagation speed within the tubing entails a time delay. Considering a tubing length of 50 cm and the physical properties of air at room temperature, the corresponding delay from the propagation is on the order of 1 ms. The spring and inertia are represented using a second-order model with the following damping ratio and natural frequency that fully characterizes the system response (Doebelin and Manik 2007).

$$\zeta = \frac{64\mu L^2}{\pi d_t^4 \sqrt{\gamma P \rho}} \sqrt{0.5 + V/V_t} \tag{1}$$

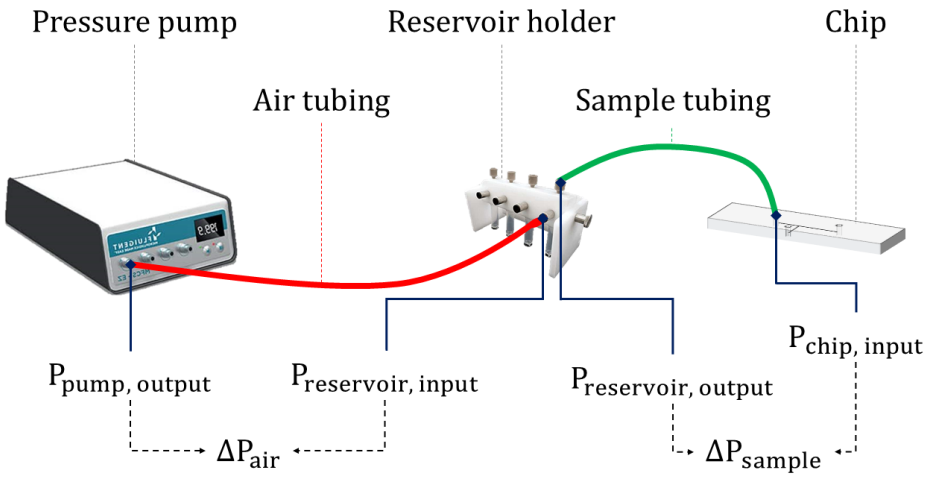

Fig. 1 Overview of the typical setup for pressure-driven flow. The focus of this study is on the difference in pressure for the air tubing (ΔP_{air}). The tubing carrying the liquid sample is already considered in the model (ΔP_{sample}) from previous work (Wong and Ren 2016; Hébert et al. 2019).

$$\omega_n = \frac{\sqrt{\gamma P/\rho}}{L\sqrt{0.5 + V/V_t}} \tag{2}$$

where ζ is the damping ratio [ ], ω_n is the natural frequency $[rad/s]$, μ is the dynamic viscosity $[kg\ m^{-1}s^{-1}]$, L is the tubing length $[m]$, d_t is the internal diameter $[m]$, γ is the heat capacity ratio [ ], P is the pressure $[Pa]$, ρ is the density $[kg\ m^{-3}]$, V is the pressure sensor dead volume $[m^3]$, and V_t is the tubing volume $[m^3]$.

Note that the dependence of the parameters on pressure means that such a lumped parameter model is valid only for small pressure changes. However, the more significant limitation in the application of this model stems from the derivation that hinges upon the rigidity of the walls. Such assumption fundamentally disagrees with the soft tubing under study.

1.3.2 Blood flow in arteries

The study of the flow of blood through our arteries couples the fluid flow with the wall deformation under pulsatile conditions from the heartbeat. Modelling and analyzing this phenomenon helps to understand the mechanism behind cardiovascular conditions for instance.

The relative scale of the arteries inner and outer diameter allows simplifying the problem by making thin-walled assumptions (Čanić et al. 2006). However, the dimensions of the air tubing do not allow such simplifications; the inner diameter and wall thickness are of the same order of magnitude. Therefore, thin-wall assumptions are deemed unreasonable.

1.3.3 System of differential equations

The air tubing can be described using a system of differential equations. The coupling between the fluid flow and the wall deformation can hence be represented (Babbs 2010). Although the equations accurately characterize the physics, the lack of simple analytical solutions renders them impractical.

$$\frac{-\partial Q}{\partial x} = \frac{\partial A}{\partial t} \tag{3}$$

$$-\frac{1}{\rho}\frac{\partial P}{\partial x} = \frac{\partial u}{\partial t} + \frac{8\pi\nu}{\rho A}u \tag{4}$$

$$P = P_{ext} + \frac{1}{C_0}\left(V - V_0 + \frac{D}{E}\frac{dV}{dt}\right) \tag{5}$$

where

$$C_0 = \frac{2\pi L r_0^3}{E h_0}, \tag{6}$$

and Q is the volumetric flow rate $[m^3 s^{-1}]$, x is the coordinate axis along the longitudinal direction $[m]$, A is the tubing cross-section area (circular) $[m^2]$, t is time $[s]$, ρ is the density $[kg\ m^{-3}]$, P is the internal pressure $[Pa]$, u is the velocity along the x direction $[m\ s^{-1}]$, ν is the dynamic viscosity $[kg\ m^{-1}s^{-1}]$, P_{ext} is the external (atmospheric) pressure $[Pa]$, V is the volume $[m^3]$, V_0 is the initial volume $[m^3]$, D is the material damping modulus $[Pa]$, E is the material elastic modulus $[Pa]$, L is the tubing length $[m]$, r_0 is the initial outer radius $[m]$, h_0 is the initial wall thickness $[m]$.

1.3.4 Thick-walled tubing deformation

The radial strain without considering the viscoelastic behaviour of the tubing (i.e. constant elastic modulus) is given in a textbook (e.g. Schmid et al. 2013).

$$\epsilon_r = \frac{P}{E}\left(\frac{r_o^2 + r_i^2}{r_o^2 - r_i^2} + \nu\right) \tag{7}$$

where ϵ_r is the radial strain [ ], P is the internal tubing pressure $[Pa]$, E is the tubing elastic modulus $[Pa]$, r_o is the outside tubing radius $[m]$, r_i is the inner tubing radius, and ν is the tubing material Poisson ratio [ ].

While a relationship between the radial strain and the inner pressure is available, the measurement of the tubing expansion is challenging with off-the-shelf strain sensors; the outer tubing diameter is only a few millimeters. A novel approach to measure strain using dispersed graphene in a soft silicone matrix was investigated (Boland et al. 2016, goophene technical note). The results were unfortunately not promising enough to further the efforts in implementing such a novel strain sensor. The signal noise and intrinsic strain sensor dynamics were the main obstacles. Furthermore, as the results will show, the tubing dynamics is of first order rather than second order. The two pressure sensors used are deemed to be sufficient for the experimental approach.

1.4 Pressure-driven flow actuation dynamics

The dynamics of the actuation system can be separated into two parts: the pump dynamics and the tubing dynamics. As conceptually illustrated in Figure 2, the pump dynamics characterizes the time response from the requested pressure (P_{req}) to the pump output ($P1$) while the tubing dynamics occurs from the pump output ($P1$) to the reservoir holder ($P2$). The reservoir holder pressure quantifies more faithfully the pressure applied to the fluid tubing inlet than the pressure at the output of the pump. Nonetheless, using the pressure pump output as the intermediary point allows analyzing the pump and tubing dynamics independently.

The tubing dynamics is investigated systematically by varying inner and outer diameters, length, material, and reservoir holder vial volume. The pump dynamics is considered for the commercial system *MFCS-EZ* available from *Fluigent* and the custom in-house pressure pump, μPump (Gao et al. 2020).

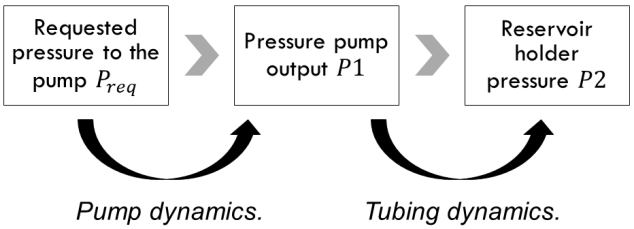

Fig. 2 Separation between pump and tubing dynamics.

1.5 Overview of this study

The objective of this study is to experimentally quantify the dynamics of the soft tubing and develop the associated models. These models can be used to predict the actual pressure applied to the microfluidic chip for fluid pumping. The availability of such models is impactful on microfluidic studies under pressure-driven flow where soft air tubing is often used to connect the pump output to the reservoir holder input (see Figure 1); the actual pressure applied to the chip is often assumed to be the pump output that is incorrect. First, a simple, yet practically useful method is presented for identifying the pressure change over the soft tubing using two pressure sensors at either end of the tubing of interest. Then, the pressure change over the soft tubing is measured under different operating conditions such as varying tubing length, material and vial volume. Following the experimental studies, a simple linear model and a nonlinear model are developed and validated to predict the system response. Finally, the performance of the models is compared and their limitations are discussed.

2 Experimental methods and materials

The *MFCS-EZ* and *μPump* can arbitrarily and independently control the pressure output at each of their outlet via a desktop computer software. The sampling rate is about 10 Hz (i.e. 100 ms period). The two pressure sensors at the two ends of the tubing respectively record simultaneously with 1 mbar accuracy every 1 ms. The data is post-processed using *Matlab* to fit a first order model.

2.1 First order model fit

The pressure data recorded provides the information about the system in the time-domain; however, the dynamics of a system is rather characterized in the frequency domain ($s \in \mathbb{C}$) and expressed as a transfer function ($G(s)$). The transfer function is the ratio of the

output ($Y(s)$) over the input ($U(s)$). A general model of the first order can be fully characterized by the scaling constant (k) and the time constant (τ). In response to a step input, the output is about 63% of the steady value after one time constant and about 98% of the steady-state value after four time constants (Close et al. 2002).

$$G(s) = \frac{Y(s)}{U(s)} = \frac{k}{\tau \cdot s + 1} \tag{8}$$

The *Matlab* function `tfest` is used to find the transfer function with no zeros and one pole (i.e. first order as per Equation 8) that best fits the data. The first order is selected because of the minimal response overshoot and to keep it simple for easier integration within control designs for instance.

2.2 Pressure sensors

2.2.1 Pressure sensor specification

The specifications for the two identical pressure sensors used are summarized in Table 1. The manufacturer datasheet accuracy is ±0.1% F.S. Therefore, in order to match the ±1 *mbar* accuracy of the *Fluigent* pump output, the range is limited to 1 bar although the pressure pump has a range up to 2 bars. Note that each pressure sensor is provided with a factory calibration to accurately convert its voltage output to gauge pressure.

The resolution of the measurements is determined by the smallest voltage increments and should be less than the targeted accuracy level. The *Arduino* communicates via a SPI protocol to an external analog-to-digital converter (ADC) with 12-bit resolution (*Microchip MCP3202*). An accurate voltage reference provides the constant 5 V supplied to the ADC (*Maxim Integrated MAX6250*). The sampling is achieved at 1 ms intervals (i.e. 1 kHz) through the use of interrupts on the *Arduino* to ensure proper and consistent data collection while continuously sending the data to the computer via USB. The 1 ms interval is selected based on the propagation of a pressure wave at the speed of sound through the media.

2.2.2 Pressure sensor location

The choice of location for the two pressure sensors aims to accurately measure the pressure at either end of the tubing. The additional components are shown in green in Figure 3. The junctions connecting the pressure sensors to the normal setup are rigid (i.e. steel). Note that a custom reservoir holder had to be manufactured to add the fourth port to measure P2. This approach was preferred than inserting a junction at one of the other reservoir holder port because of its lesser impact on the flow.

The minimum time resolutions of the junctions added to the system are thoroughly assessed. Details are presented in the supplementary material S1. Based on the results of the assessment, the minimum time constant that can confidently be investigated using the junctions is 10 ms.

Table 1 Specification summary for the pressure sensors (*TE Connectivity U536D-H00015-001BG*).

Range	0 to 1 bar
Accuracy	± 1 mbar
Resolution	0.24 mbar
Sampling	1 kHz

2.3 Tubing materials and dimensions

The various tubing materials and dimensions investigated are summarized in Table 2. The microfluidic pressure pumps and reservoir holder typically use barbed connections. The *MFCS-EZ* from *Fluigent* comes equipped with 1 X 3 mm tubing. Nonetheless, the barbed connections are also functional for the closest imperial equivalent that has an inner diameter of 1/16" (∼1.59 mm). The variety of materials for the metric size is more restricted. Hence, the different materials are investigated in the imperial size only.

The elastic modulus of each material is experimentally determined using a straightforward approach with a ruler and suspended weights. The details and the plot are presented in the supplementary material S2.

3 Results and discussion

As shown in Figure 2, the system dynamics can be separated into the pump dynamics and the tubing dynamics. The results supporting this separation are presented in the supplementary material S3. The rest of the results is separated into these two main sections before addressing model validation, and finally, limitations.

3.1 Pump dynamics

The control strategy previously implemented neglects the dynamics introduced by the soft tubing and the actuation when adjusting the requested pressure (Wong and Ren 2016). The controller design relied solely on

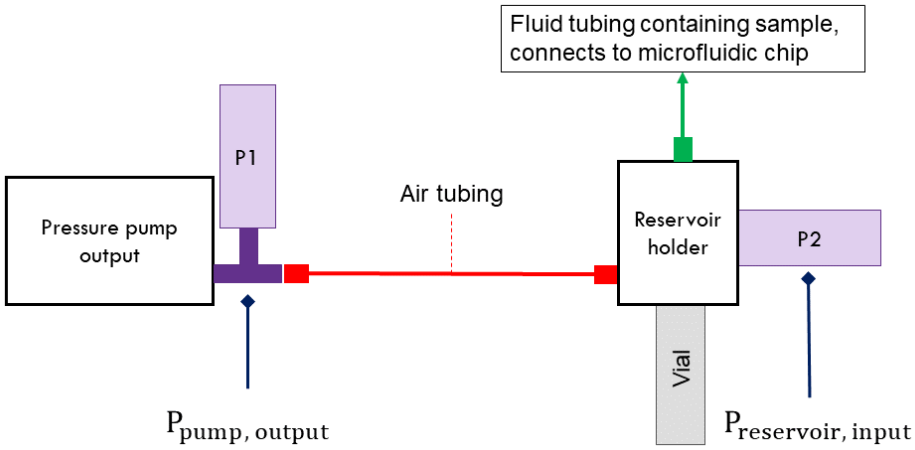

Fig. 3 Experimental setup to measure the impact of the air tubing dynamics (ΔP_{air}). Two pressure sensors are strategically located to measure the pressure at either end of the air tubing with minimal impact.

Table 2 Details of the materials and dimensions of the various tubing.

inner X outer diameter	Wall thickness	Material label	E(1) [MPa]	Lengths [cm]
1 X 3 mm	1 mm	Medium silicone	4	20.4, 30.2, 30.1, 50.3, 66.5
1/16" X 1/8" (1.59 X 3.18 mm)	1/32" (0.79 mm)	Soft silicone	1	66.5
		Medium silicone	4	66.5
		Hard Tygon	7	66.5

(1) Elastic modulus. See Figure S2.1 for experimental strain-stress curve with linear fit. Uncertainties: $\pm 0.5\ MPa$.

the model of the plant (i.e. the microfluidic chip and fluid tubing), hence excluding the pump and air tubing. The requested pressure to the pump was assumed to instantly correspond to the pressure at the fluid tubing inlet in the vial at the reservoir holder. These dynamics were shown to be reasonably neglected for the current running rate of the system at 10 Hz. Nevertheless, better understanding the short-term actuation dynamics is critical to increasing the controller performance; furthermore, increasing the system sampling rate would magnify the impact of the short-term actuation dynamics and challenge the controller performance.

Note that there are limitations due to the "black-box" nature of commercial products such as *Fluigent*'s *MFCS-EZ*. Moreover, the implementation of such active control platform on regular desktop computers limits the consistency of the actuation delay due to scheduling handled by the operating system (*Windows*). The pump dynamics is determined as per Equation 8. The input is the requested pressure and the output is the pump output pressure ($P1$).

3.1.1 Fluigent

The commercial nature of the *Fluigent MFCS-EZ* pump restricts the information available concerning both the internal components as well as the controller. Consequently, it is treated as a black-box for which the requested pressure is the input and the provided pressure is the output.

The first order model is observed to match the response fairly well for certain pressures. However, the time constant varies with respect to the pressure and displays significant hysteresis effects in the lower pressure range (see Figure 4). Moreover, at high pressures, the first order model (or even a second order model) differs significantly from the response. Note that as the pressure output will eventually match the requested pressure, the scaling constant (k) is set to one.

3.1.2 µPump

In contrast to the lack of information available for black-box commercial systems such as the *Fluigent* pump, µPump is a customized system designed and built in-house. All details pertaining to the hardware and the software are available (Gao et al. 2020). The pressure output is controlled by the internal circuit of the *ControlAir* E/P transducer (*T900-CIM*).

The response follows more closely a second order system than a first-order system due to the better defined oscillations. Nonetheless, there appears to be a

relatively slow integral component for the closed-loop controller. Thus, although the output pressure rapidly approaches the requested pressure, there is a noticeable period where the steady-state error is slowly eliminated through the integral component. Hence, the second order model somewhat differs from the μPump dynamics. A crude simplification can be made to simply represent the delay in achieving the requested pressure using a first order model. Considering that the pump will achieve its target output pressure, the scaling constant value is set to one while the time constant is shown in Figure 5. Similarly to the *Fluigent* pump, there is significant hysteresis effects present. However, the overall behaviour is much more constant over the pressure range. Moreover, the time constant is also generally smaller for μPump compared to *Fluigent*.

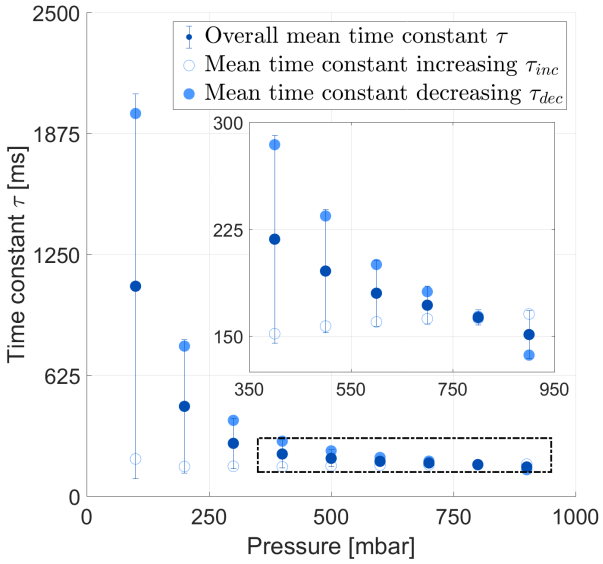

Fig. 4 Time constant (τ) variations with pressure for the *Fluigent MFCS-EZ* pump. The error bars represent $\pm$ 1 standard deviation from the overall mean time constant.

3.2 Tubing dynamics

The previous section concerning the pump dynamics is mainly pertinent within the context of active microfluidics. The tubing dynamics, on the other hand, is relevant to both passive and active microfluidics. The tubing dynamics is determined as per Equation 8. The input is the pump output pressure ($P1$), and the output is the tubing end at the reservoir holder inlet ($P2$).

3.2.1 Pressure variations

As previously indicated by the literature about unsteady pressure measurement, the dynamic behaviour of the tubing is expected to depend on pressure.

The scaling constant (k) exhibits dependence on the pressure as shown in Figure 6(a); however, there is no significant difference whether the pressure is increasing or decreasing. As opposed to the time constant that considers short term transients, the scaling constant characterizes the steady state that is less prone to hysteresis effects. The value is close to but slightly less than one. This is attributed to the pressure difference between the tubing ends that is required to drive the flow. Considering that the difference in pressure is proportional to flow rate (Bruus 2008), the value of the scaling constant (k) is expected to decrease with increasing flow.

For the metric 1X3 mm tubing, the time constant variations with pressure are shown in Figure 6(b) for both increasing and decreasing pressure. The time constant for increasing pressure is consistently larger than the one for decreasing pressure. This is attributed to the compliance of the tubing. When the pressure is increased, part of the air flows in the outward radial direction to rationalize the increase in diameter. Moreover, from an energy analysis perspective, the expansion of the tubing requires some energy that is then stored as elastic energy in the expanded tubing. When the pressure is decreased, the tubing contracts back to a smaller diameter. The elastic energy that was stored

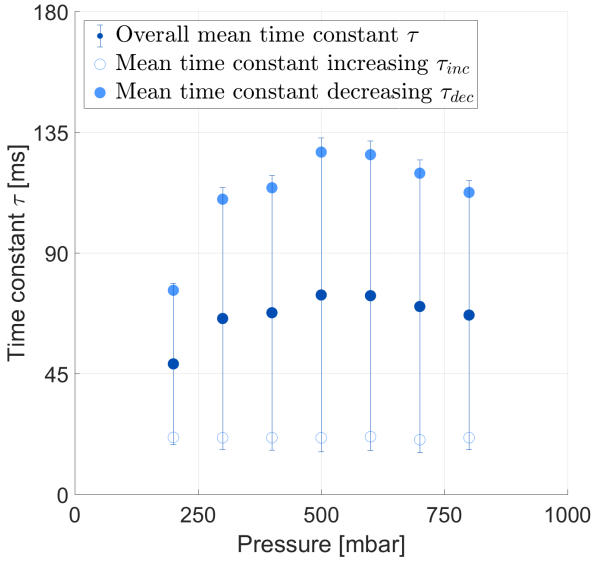

Fig. 5 Time constant (τ) variations with pressure for *μPump*. The error bars represent $\pm$ 1 standard deviation from the overall mean time constant.

in the wall is transferred back to the flow. Thus, the energy exchange from the flow to the wall elasticity and vice versa results in hysteresis effects for the time constant (τ).

For the imperial tubing, different tubing materials are investigated. However, the dynamics is too fast to be captured accurately by the experimental setup, as shown in Figure 7. All materials exhibited a behaviour with time constants less than 10 ms. Compared to the metric tubing, both the inner diameter and wall thickness vary due to the restricted availability of sizes; nonetheless, the faster dynamics is attributed to the larger inner diameter rather than the thinner wall. The wall thickness influences the tubing expansion and hence, the change with respect to pressure; the nominal starting inner diameter at zero pressure determines the time constant scale. Figure 6 shows such decreasing time constant value with increasing diameter (i.e from the increased expanded tubing diameter).

3.2.2 Length variations

The time constant is expected to get smaller with the tubing length. The longest length of 66.5 cm for the imperial tubing has a time constant already too small to accurately quantity; thus, only the metric tubing is considered henceforth. The results of the linear fit for the tubing time constant for different lengths are presented in Figure 8. The scaling constant is not significantly affected by the change in length and thus is omitted.

The details of the linear fit are included in Table 3. The general trend is for the time constant to increase with increasing length as expected.

3.2.3 Vial volume variations

Similarly to the length variations, the vial volume variations only take into account the metric tubing. The vial attached to the reservoir holder contains the sample to be injected into the microfluidic chip. The small quantities required to perform the manipulations at the microfluidic scale entails small changes of the sample volume in the vial. However, variations over long periods of time as well as in the initial volume when filling the vial can potentially lead to changes in the dynamics. The significance of these changes is herein assessed.

The different volumes investigated for the vial are approximately: 0.3 ml, 1 ml, and 2 ml. The results for length variations previously presented all considered the 2 ml vial volume (i.e. empty vial). The relationship for the scaling constant k does not vary significantly with volume. However, the time constant relationship does change more significantly depending on the volume of the vial. Nevertheless, the change of the time constant over the full volume and pressure range is reasonably small. The linear fit is mainly at the same time constant scale as shown in Figure 9. Hence, volume variations are neglected.

3.2.4 Tubing dynamics results summary

The experimental setup can only confidently quantify tubing dynamics with a time constant larger than 10 ms. All results for the 1/16"X1/8" tubing are faster; hence, they are not quantified. Nonetheless, such fast dynamics is considered to be negligible within the microfluidic pump context. Consequently, only the dynamics for the 1X3 mm tubing are herein summarized. Generally, the value for the scaling constant (k) is considered constant as it weakly depends on pressure.

As for the time constant (τ), the results for the different lengths and volumes are summarized in Table 3. As previously mentioned, although there are some variations for different vial volumes (over the 1.7 ml range), they are deemed negligible. The overall tubing length affects much more significantly the time constant. Furthermore, the tubing length can easily be measured and maintained constant whereas the vial volume is expected to vary while the experiments are performed.

3.3 Validation

3.3.1 Repeatability for k and τ

The repeatability of the experimental quantification of the scaling and time constants is assessed by alternating between two pressures. The data is averaged over three datasets each consisting of 10 increasing steps and 10 decreasing step responses. The repeated results are summarized in Tables 4 and 5.

The data obtained from the successive steps (previously in Figure 6, the first two data points) is compared against the results of the repeated test. The time constant all match within the time resolution of the system (i.e. 1 ms). The scaling constant shows more variations between the single and repeated data for the 200 mbar setpoint. However, the discrepancy is within 3%; therefore, it is not considered significant.

3.3.2 Model verification

Two models are used for verification: linear and nonlinear.

The linear model (Equation 8) depends solely on two parameters: the scaling constant (k) and the time

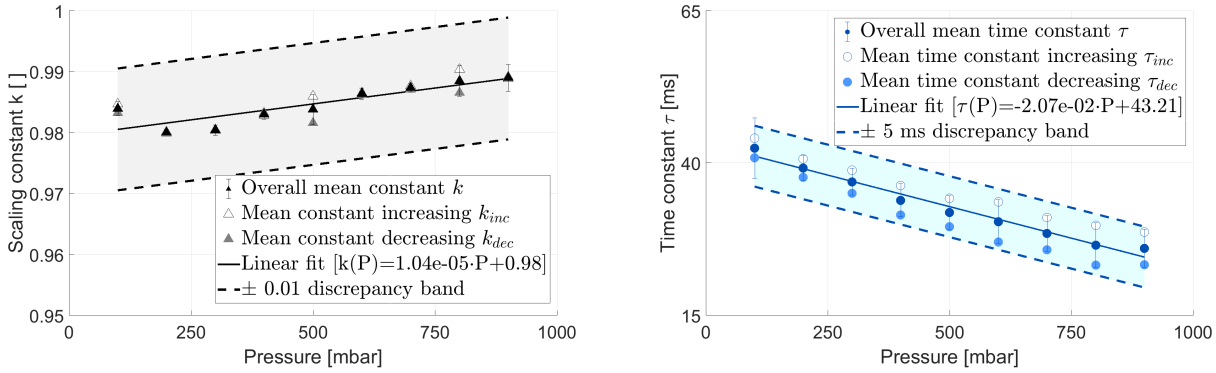

(a) Scaling constant k. (b) Time constant τ.

Fig. 6 Experimental quantification of first order dynamics over the pressure range for the 1X3 mm medium silicone tubing of 66.5 cm length and 2 ml vial volume. The trend of the decreasing and increasing data shows the hysteresis effects. The time constant is consistently smaller for decreasing pressure compared to increasing pressure. The error bars represent ± 1 standard deviation from the overall mean constant.

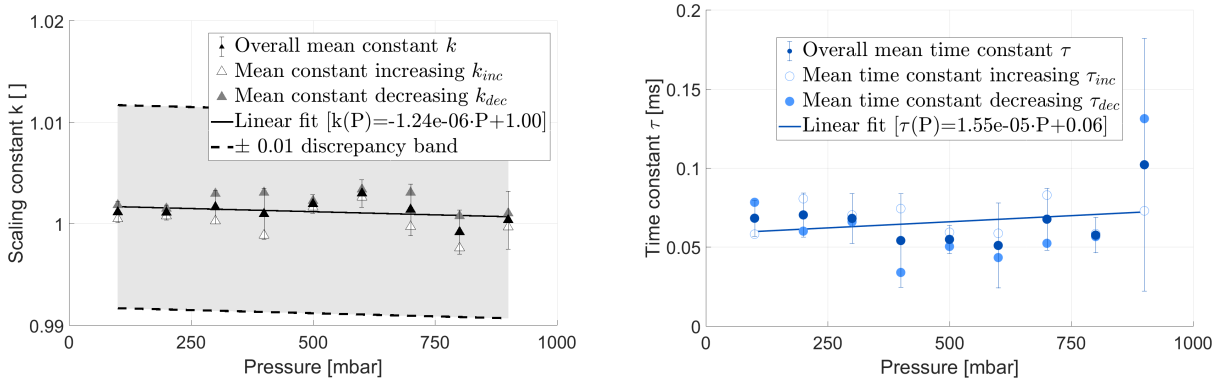

(a) Scaling constant k. (b) Time constant τ.

Fig. 7 Experimental quantification of first order dynamics over the pressure range for the 1/16"X1/8" medium silicone tubing of 66.5 cm length and 2 ml vial volume. Similar results are obtained for all three materials (Table 2). The time constant is too small to accurately quantify with the current experimental setup. The error bars represent ± 1 standard deviation from the overall mean constant.

constant (τ). The two values are constants determined by averaging over the pressure range. The nonlinear model uses the linear fit to determine the value of the two parameters (k and τ) based on the pressure. The sensitivity of the scaling constant (k) to pressure changes is weak while the sensitivity of the time constant (τ) is more significant. The difference between the input and output pressure is fairly small at all time; furthermore, the linear relationship is fairly shallow. Therefore, the pressure used for the nonlinear model is taken as the mean of the input and output pressure ($P1$ and $P2$). This average pressure is used to calculate the time constant based on the linear fit from Table 3. The scaling constant is considered constant at its mean value. Equation 9 shows how the linear equation for the time constant ($\tau(x,u)$) is included in the linear model structure.

$$\dot{x} = \begin{bmatrix} \frac{-1}{\tau(x,u)} \end{bmatrix} x + \begin{bmatrix} \frac{k}{\tau(x,u)} \end{bmatrix} u$$

$$\dot{x} = f(x,u) = \left(\frac{-1}{a_\tau \cdot \bar{P} + b_\tau} \right) x + \left(\frac{k}{a_\tau \cdot \bar{P} + b_\tau} \right) u \quad (9)$$

where $\dot{x}$ is the derivative of the state vector, $x = \begin{bmatrix} P2 \end{bmatrix}$ is the state vector, $u = \begin{bmatrix} P1 \end{bmatrix}$ is the input, $\tau(x,u) = a_\tau \cdot \bar{P} + b_\tau$ is obtained from the linear fit parameters from Table 3, $\bar{P}$ is the mean of u and x (i.e. $P1$ and $P2$), and k is the scaling constant.

Simulink is used to simulate the nonlinear system (Equation 9). However, expressing such a nonlinear system concisely within the context of controller design is challenging. Hence, a pragmatic approach instead uses

Table 3 Summary of the variations in the time constant (τ) depending on tubing length (Figure 8) and vial volume (Figure 9) for 1X3 mm tubing.

Tubing length [cm]	**Vial volume [ml]**	**Time constant $\tau(P)$ $[ms]$**	
		$a_\tau^{(1)}$ $[ms \cdot mbar^{-1} \times 10^{-3}]$	$b_\tau^{(2)}$ $[ms]$
$20.4^{(3)}$	2	-9.37	8.9
30.2	2	-14.5	20.2
40.1	2	-8.11	24.0
50.3	2	-14.0	31.9
66.5	2	-20.7	43.2
66.5	1	-19.7	38.9
66.5	0.3	-11.3	32.3

(1) a_τ is the slope of the linear fit.

(2) b_τ is the intercept of the linear fit.

(3) The associated dynamics are too fast to reliably quantify.

Table 4 Repeatability summary for 100 mbar pressure set point.

	Scaling constant (k) [ ]			**Time constant (τ) [ms]**		
	mean	*inc.*	*dec.*	*mean*	*inc.*	*dec.*
Single data	0.9755	0.9754	0.9755	41	44	38
Repeated data	0.9760	0.9760	0.9759	42	44	39

Table 5 Repeatability summary for 200 mbar pressure setpoint.

	Scaling constant (k) [ ]			**Time constant (τ) [ms]**		
	mean	*inc.*	*dec.*	*mean*	*inc.*	*dec.*
Single data	0.9593	0.9595	0.9592	40	41	38
Repeated data	0.9834	0.9835	0.9833	41	42	39

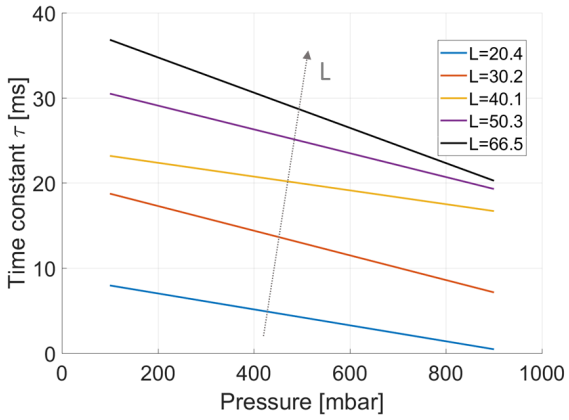

Fig. 8 Summary of the time constant (τ) fit for different lengths. Tubing dimensions of 1X3 mm. The detailed data is presented in Table 3.

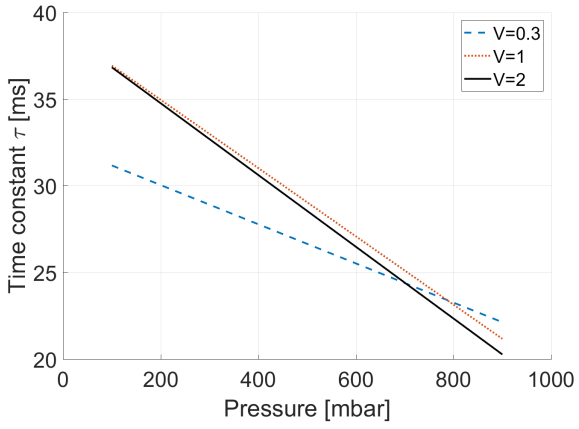

Fig. 9 Summary of the time constant (τ) fit for different volumes (ml). Tubing dimensions of 1X3 mm. The detailed data is presented in Table 3.

the simple linear first order with constant parameters for controller design.

A different and more diverse pressure signal is used to assess model validity. The prediction of the full non-linear relationship is compared to the simpler first-order linear model. The performance for the prediction is assessed using the mean square error (MSE) and the maximum error between the predicted and actual pressure output ($P2$).

$$MSE = \frac{1}{n}\sum_{i=1}^{n}(P2_i - \hat{P2}_i)^2 \quad (10)$$

where MSE is the mean square error $[mbar^2]$, n is the number of data points [ ], $P2_i$ is the measured pressure at the reservoir holder for the i^{th} datapoint $[mbar]$, and $\hat{P2}_i$ is the predicted pressure at the reservoir holder for the i^{th} datapoint based on the measured $P1$ $[mbar]$.

Figure 10 shows the validation signal as well as the prediction for both the linear and nonlinear model with their corresponding error. This is specifically for the 1X3 mm tubing that is 66.5 cm long and with the 2 ml vial. The slightly larger *MSE* and maximum error for the linear model compared to the nonlinear model demonstrates the small performance decrease that must be conceded for the simpler model. Furthermore, the difference between the two pressure sensor measurements represent the assumption that the pressure instantly propagates without any modelling involved; the *MSE* and maximum error are both much more significant than either of the models. Therefore, the use of the model, albeit with some assumptions and simplifications, still nevertheless improves the accuracy of the reservoir holder pressure prediction.

The first order linear model performance for each case is summarized in Table 6. Their respective parameter taken as the mean are also included. Note that for the various volumes for the 66.5 cm long tubing, the same parameters are used. Nevertheless, the prediction from the model still outperforms the absence of model. Hence, this confirms the validity of the model even with varying volume, only the tubing length should be considered when determining the scaling and time constant parameter values.

3.4 Limitations

In general models do not aim to fully and exactly describe a system with 100% accuracy in all circumstances. The objective is rather to develop a mathematical representation of the system with *sufficient* accuracy under certain operating conditions. In this study, the linear model is validated for pressures between 0 and 1 bar; the linear model is hence meant to be used for a pressure range from 0 to 1 bar. The pressure from the pump is changed every 100 ms (10 Hz).

The maximum actuation frequency of 10 Hz is of special note because of its larger value than the time constant range identified. The variations in time constant with pressure are likely to impact more the prediction error for a faster pressure actuation. However, the current setup frequency is mainly limited by the *Fluigent* pump proprietary software and the μPump E/P transducer.

The tubing length is limited between 20.4 cm and 66.5 cm as this corresponds to the range investigated. Moreover, the vial volume is varied only between 0.3 ml to 2 ml. The only tubing dimensions are 1X3 mm although other conclusions are drawn for the larger 1/16"X1/8" tubing that exhibited a response too fast for the measuring apparatus. Finally, although different tubing materials were investigated for the 1/16"X1/8" tubing, no conclusive quantification could be extracted from the results. Only the soft silicone tubing was considered for the 1X3 mm as it is the most widely available materials for these tubing dimensions.

4 Conclusion

4.1 Summary

The dynamics investigation is mainly pertinent within the context of active microfluidics; short-term oscillations are much less important than long-term behaviour and stability for passive microfluidics. Nonetheless, examining the dynamics of the pump and the tubing is beneficial for both active and passive microfluidics.

On one hand, passive microfluidics aims for stability and dampened short-term oscillations that can be provided by a longer, smaller inner diameter tubing. On the other hand, active microfluidics benefits from shorter delays for the propagation of the pressure from the pump output to the reservoir holder provided by shorter and slightly bigger tubing that is the imperial tubing with 1/16" inner diameter. The dynamics of the 1X3 mm tubing for various lengths operated between pressures of 0 bar to 1 bar and volumes from 0.3 ml to 2 ml can be approximated using a first-order model; the parameters are summarized in Table 6. Such a first-order linear model is shown to improve the prediction error comparatively to the absence of any model. Moreover, the complexity of the nonlinear model only marginally improved the performance and hence, is deemed unnecessary.

4.2 Future work

The relationship between the pump output and reservoir holder pressure can be included within the previous control design strategy (Wong and Ren 2016) to enhance performance. The addition of the dynamics introduced by the pump response time as well as the pressure propagation through the tubing hence would eliminate

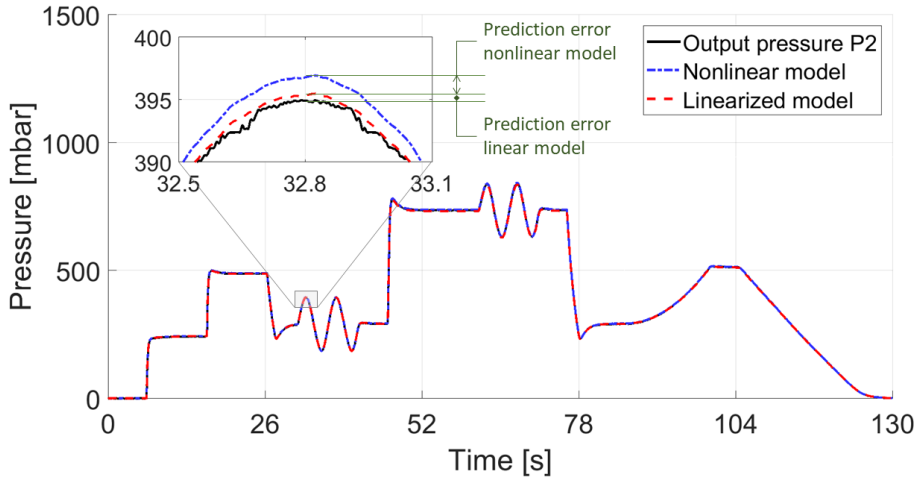

(a) Output pressure P2 from the measurement, nonlinear model, and linear model.

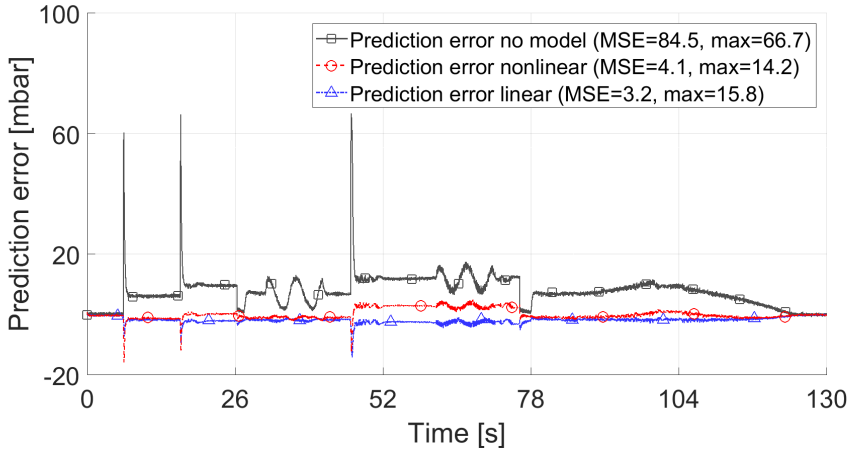

(b) Prediction error for the output pressure P2 without a model (P2 = P1), with the nonlinear model, and with the linear model.

Fig. 10 Model validation and comparison between no model, the nonlinear model and the simple linear model simulations. The similar MSEs show that there is not significant prediction error improvement for the more complex nonlinear model compared to the simpler linear model. (1X3 mm tubing, 66.5 cm long, 2 ml vial). Either model significantly improves upon the no-model prediction.

the previously built-in assumption that the pressure requested is applied instantaneously to the sample tubing inlet. The consideration of the pump and air tubing dynamics can be achieved by arranging the subsystems in series: pump, air tubing, and microfluidic chip. For the state-space modelling, this results in matrix concatenation.

The improved model that considers the air tubing can be leveraged in a grey-box system identification study. Briefly, the grey-box system identification fixes the model structure–including the air tubing–to maintain physical meaning of the identified parameters. The system identification algorithm requires the input (pressure) and output (droplet position) to be recorded while a droplet moves within the channel. The model structure used is essential to the quality of the results obtained. The inclusion of the tubing dynamics within the model is envisioned to enable a better description of the physical system. Thus, the results obtained from the system identification algorithm would be more narrowly distributed.

Furthermore, a more detailed analysis of the behaviour of the two different pumps would help to determine a model describing their behaviour better than the crude first order linear model herein presented. The behaviour could be better represented by a second order system for instance. Increasing the complexity would enable a more accurate model. Moreover, the signifi-

Table 6 Performance for each first order linear model for the mean parameter values based on length compared against the no-model performance.

Tubing length [cm]	Vial volume [ml]	Linear model		Performance criteria	
		k	τ	$MSE^{(1)}$ $[mbar^2]$	$e^{(2)}_{max}$ $[mbar]$
20.4 (3)	2	0.99	4	1.6	17.9
30.2	2	0.99	13	2.3	12.6
40.1	2	0.98	20	3.0	12.4
50.3	2	0.99	25	3.8	15.9
66.5	2	0.98	33	3.2	15.8
66.5	1	0.98	33	18.2	11.4
66.5	0.3	0.98	33	21.0	11.2
66.5(4)	2	–	–	84.5	66.7

(1) MSE is mean squared error as per Equation 10.

(2) e_{max} is the maximum error over the validation data.

(3) The associated dynamics are too fast to reliably quantify.

(4) No-model performance. (i.e. $\hat{P2} = P1$).

cant hysteresis could be taken into account rather than averaged out.

Author contributions

MH participated in the conceptualization, data curation, formal analysis, investigation (performing the experiments), methodology, project administration, supervision of WB, software development, validation, and writing (at all stages).

WB contributed to the software and resources used for the experiments, more specifically, the pressure measurement apparatus and custom reservoir holder manufacturing.

JPH participated in the conceptualization, methodology, and the review and editing of the manuscript.

CLR participated in the manuscript review and editing, conceptualization, project administration, and supervision of both MH and WB. CLR also led the funding acquisition.

Acknowledgements

The authors acknowledge the funding provided by NSERC in the form of grants supplied to Prof. Carolyn Ren and scholarships awarded to Marie Hébert and William Baxter.

Conflict of interest

The authors declare that they have no conflict of interest.

References

S. Atabakhsh and S. J. Ashtiani. Thermal actuation and confinement of water droplets on paper-based digital microfluidics devices. *Microfluidics and Nanofluidics*, 22(4):43, 2018.

M. Azizi, M. Zaferani, S. H. Cheong, and A. Abbaspourrad. Pathogenic bacteria detection using rna-based loop-mediated isothermal-amplification-assisted nucleic acid amplification via droplet microfluidics. *ACS sensors*, 2019.

C. F. Babbs. Behavior of a viscoelastic valveless pump: a simple theory with experimental validation. *Biomedical engineering online*, 9(1):42, 2010.

P. Bodénès, H.-Y. Wang, T.-H. Lee, H.-Y. Chen, and C.-Y. Wang. Microfluidic techniques for enhancing biofuel and biorefinery industry based on microalgae. *Biotechnology for biofuels*, 12(1):33, 2019.

C. S. Boland, U. Khan, G. Ryan, S. Barwich, R. Charifou, A. Harvey, C. Backes, Z. Li, M. S. Ferreira, M. E. Möbius, et al. Sensitive electromechanical sensors using viscoelastic graphene-polymer nanocomposites. *Science*, 354(6317):1257–1260, 2016.

H. Bruus. *Theoretical microfluidics*, volume 18. Oxford university press Oxford, 2008.

S. Čanić, J. Tambača, G. Guidoboni, A. Mikelić, C. J. Hartley, and D. Rosenstrauch. Modeling viscoelastic behavior of arterial walls and their interaction with pulsatile blood flow. *SIAM Journal on Applied Mathematics*, 67(1):164–193, 2006.

C. M. Close, D. K. Frederick, and J. C. Newell. *Modeling and analysis of dynamic systems*, volume 3. Wiley New York, NY, 2002.

H. J. Crabtree, J. Lauzon, Y. C. Morrissey, B. J. Taylor, T. Liang, R. W. Johnstone, A. J. Stickel, D. P. Manage, A. Atrazhev, C. J. Backhouse, et al. Inhibition of on-chip pcr using pdms–glass hybrid microfluidic chips. *Microfluidics and nanofluidics*, 13(3):383–398, 2012.

E. O. Doebelin and D. N. Manik. Measurement systems: application and design. 2007.

R. Z. Gao, M. Hébert, J. Huissoon, and C. L. Ren. μpump: An open-source pressure pump for precision fluid handling in microfluidics. *HardwareX*, 7:e00096, 2020.

T. Glawdel and C. L. Ren. Global network design for robust operation of microfluidic droplet generators with pressure-driven flow. *Microfluidics and nanofluidics*, 13(3):469–480, 2012.

M. Hébert, M. Courtney, and C. L. Ren. Semi-automated on-demand control of individual droplets with a sample application to a drug screening assay. *Lab on a Chip*, 2019.

C.-A. Kieffer, S. Ritty, T. Boudot, N. Petit, J. Weber, and A. Le Nel. A high-precision fluid handling system based on pressure actuation: multi-inlets flow rate control. In *Proc. 3rd Eur. Conf. Microfluidics*, volume 252, 2012.

P. M. Korczyk, O. Cybulski, S. Makulska, and P. Garstecki. Effects of unsteadiness of the rates of flow on the dynamics of formation of droplets in microfluidic systems. *Lab on a Chip*, 11(1):173–175, 2011. doi: 10.1039/c0lc00088d.

M. Rasponi, A. Gazaneo, A. Bonomi, A. Ghiglietti, P. Occhetta, G. B. Fiore, A. Pessina, and A. Redaelli. Lab-on-chip for testing myelotoxic effect of drugs and chemicals. *Microfluidics and Nanofluidics*, 19 (4):935–940, 2015.

S. R. Schmid, B. J. Hamrock, and B. O. Jacobson. *Fundamentals of machine elements*. CRC Press, 2013.

J. Wang, M. Jin, Y. Gong, H. Li, S. Wu, Z. Zhang, G. Zhou, L. Shui, J. C. Eijkel, and A. Van Den Berg. Continuous fabrication of microcapsules with controllable metal covered nanoparticle arrays using droplet microfluidics for localized surface plasmon resonance. *Lab on a Chip*, 17(11):1970–1979, 2017a.

J. Wang, Y. Li, X. Wang, J. Wang, H. Tian, P. Zhao, Y. Tian, Y. Gu, L. Wang, and C. Wang. Droplet microfluidics for the production of microparticles and nanoparticles. *Micromachines*, 8(1):22, 2017b.

D. Wong and C. L. Ren. Microfluidic droplet trapping, splitting and merging with feedback controls and state space modelling. *Lab on a Chip*, 16(17): 3317–3329, 2016.

Figure 1 Overview of the typical setup for pressure-driven flow. The focus of this study is on the difference in pressure for the air tubing (ΔP_{air}). The tubing carrying the liquid sample is already considered in the model (ΔP_{sample}) from previous work (Wong and Ren 2016; Hébert et al. 2019).

Figure 2 Separation between pump and tubing dynamics.

Figure 3 Experimental setup to measure the impact of the air tubing dynamics (ΔP_{air}). Two pressure sensors are strategically located to measure the pressure at either end of the air tubing with minimal impact.

Figure 4 Time constant (τ) variations with pressure for the *Fluigent MFCS-EZ* pump. The error bars represent $\pm$ 1 standard deviation from the overall mean time constant.

Figure 5 Time constant (τ) variations with pressure for *μPump*. The error bars represent $\pm$ 1 standard deviation from the overall mean time constant.

Figure 6 Experimental quantification of first order dynamics over the pressure range for the 1/16"X1/8" medium silicone tubing of 66.5 cm length and 2 ml vial volume. Similar results are obtained for all three materials (Table 2). The time constant is too small to accurately quantify with the current experimental setup. The error bars represent $\pm$ 1 standard deviation from the overall mean constant.

Figure 6(a) Scaling constant k.

Figure 6(b) Time constant τ.

Figure 7 Experimental quantification of first order dynamics over the pressure range for the 1/16"X1/8" medium silicone tubing of 66.5 cm length and 2 ml vial volume. Similar results are obtained for all three materials (Table 2). The time constant is too small to accurately quantify with the current experimental setup. The error bars represent $\pm$ 1 standard deviation from the overall mean constant.

Figure 7(a) Scaling constant k.

Figure 7(b) Time constant τ.

Figure 8 Summary of the time constant (τ) fit for different lengths. Tubing dimensions of 1X3 mm. The detailed data is presented in Table 3.

Figure 9 Summary of the time constant (τ) fit for different volumes (ml). Tubing dimensions of 1X3 mm. The detailed data is presented in Table 3.

Figure 10 Model validation and comparison between no model, the nonlinear model and the simple linear model simulations. The similar MSEs show that there is not significant prediction error improvement for the more complex nonlinear model compared to the simpler linear model. (1X3 mm tubing, 66.5 cm long, 2 ml vial). Either model significantly improves upon the no-model prediction.

Figure 10(a) Output pressure P2 from the measurement, nonlinear model, and linear model.

Figure 10(b) Prediction error for the output pressure P2 without a model (P2 = P1), with the nonlinear model, and with the linear model.